

Optically-isolated millimeter-wave detector for the Toroidal Plasma Experiment

M. Baquero-Ruiz,¹ S. Alberti,¹ O. Chellai,¹ I. Furno,¹ T. Goodman,¹ F. Manke,¹ P. Micheletti,¹ G. Plyushchev,¹ and A.K. Skrivervik²

¹*École Polytechnique Fédérale de Lausanne (EPFL), Swiss Plasma Center (SPC), CH-1015 Lausanne, Switzerland*

²*École Polytechnique Fédérale de Lausanne (EPFL), Microwaves and Antennas Group (MAG), CH-1015 Lausanne, Switzerland*

(Dated: 13 November 2018)

We have designed and built an optically-isolated millimeter-wave detection system to prevent interference from a nearby, powerful, 2.45 GHz microwave source in millimeter-wave propagation experiments in the TORoidal Plasma Experiment (TORPEX). A series of tests demonstrates excellent system noise immunity and the ability to observe effects that cannot be resolved in a setup using a bare Schottky diode detector.

I. INTRODUCTION

Millimeter waves (mmw) are electromagnetic (EM) waves with wavelength approximately in the range $\approx 1 - 10$ mm, which in free-space corresponds to frequencies $\approx 30 - 300$ GHz. These types of waves have applications in many different branches of science and engineering, including astrophysics¹, telecommunications², radar systems³ and medicine⁴. In plasma physics, mmws are widely used in diagnostic systems such as interferometers⁵ as well as for plasma heating in fusion-grade tokamaks⁶. At present, there is significant interest in gaining understanding on the propagation of mmws in turbulent plasmas^{7,8}, as it may have important implications in the deposition of heating power and current drive efficiency in fusion experiments⁹.

Schottky diode detectors (SDD) provide a simple means of detecting mmws⁵. When operating in square-law regime^{5,10}, SDDs produce a voltage proportional to the input mmw power. The response is very wide-band, making SDDs very convenient for general purpose detection. Furthermore, some SDDs are zero-bias, requiring no additional biasing to operate. These types of SDD are particularly well suited for detection of mmws in areas of limited access since they can work essentially standalone. Indeed, the only connection that they require is from the output to the read-out electronics.

In the TORoidal Plasma Experiment (TORPEX^{11,12}) we installed a zero-bias SDD to detect a ≈ 30 GHz mmw beam that is made to traverse a turbulent plasma. The plasma is generated and sustained with a separate magnetron that produces heating microwaves (HW) at a frequency $f_{\text{heat}} = 2.45$ GHz with typical power $P_{\text{heat}} = 100 - 1000$ W. In early trials, it was observed that the activation of HWs strongly affected the SDD despite the mmw receiver having been designed to block EM waves at the lower HW frequencies (Sec. II). Noise in the SDD output signal reached an unacceptable level for experiments whose aim was to distinguish fluctuations in the detection of the ≈ 30 GHz mmw beam⁸.

Efforts at better shielding the SDD showed only limited improvement. The experimental setup allows differ-

ent types of EM coupling^{13,14} which make it possible for magnetron-related noise or spurious power from HWs to couple to the SDD and produce an unwanted response. The identification of the noise paths, nevertheless, proved to be extremely challenging, especially because the wide-band character of the SDD prevents narrowing the search to specific frequencies. Use of a different approach to detect mmw-beam fluctuations with a heterodyne system⁵ was unsuccessful, as HWs were also seen to strongly affect the measurements. Instead, we built an optically-isolated mmw detector, based on a zero-bias SDD, as an alternative to alleviate the effect of HWs on mmw detection (Sec. III). The capabilities of the system are demonstrated with a set of measurements and comparisons to data obtained using a bare SDD (Sec. IV).

Although the detector is developed in a plasma physics context, the design may be of interest in other areas of science and engineering where SDDs are used for mmw detection, and where pickup from nearby, powerful, ~ 2.4 GHz microwave sources raises concern.

II. TORPEX AND MMW EXPERIMENTAL SETUP

TORPEX^{11,12} (Fig. 1) is a toroidal plasma device located at the Swiss Plasma Center in Lausanne, Switzerland. With a major radius $R = 1$ m and minor radius $a = 20$ cm, TORPEX is used in basic studies of magnetized plasmas of hydrogen (or other gases^{11,12}) with typical particle densities $10^{15} - 10^{17} \text{ m}^{-3}$, electron temperatures $1 - 5$ eV and plasma potentials $10 - 20$ V. The discharges are produced and sustained by absorption of the 2.45 GHz HWs at the electron-cyclotron and upper-hybrid resonances¹⁵. In the typical Simple Magnetized Torus (SMT) configuration, the magnetic field has a small vertical component $B_z \leq 5$ mT and a dominant toroidal component $B_\phi \approx 70$ mT. SMT plasmas exhibit turbulent features that are well suited for studies of turbulent plasma structures^{11,12,16}.

HWs are generated using a Muegge MH050KS-310BN magnetron head. In our experiments, we only consider $P_{\text{heat}} \leq 600$ W and continuous discharges of duration

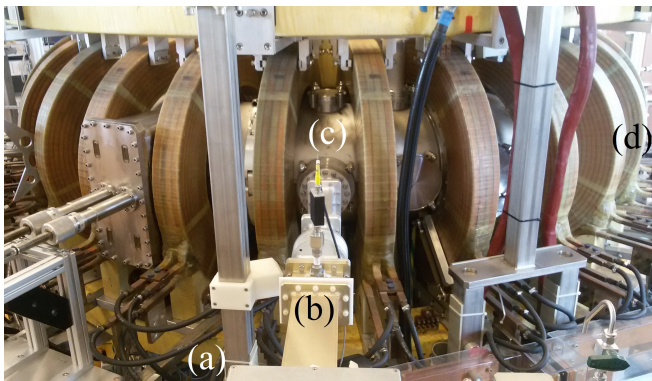


FIG. 1. The TORPEX device viewed from the magnetron head. The output end of the magnetron (a) is visible in the foreground. (b) HW transmission line. The transmitted HW power is measured near the step twist. (c) TORPEX stainless steel toroidal vessel. The coils surrounding it are used to generate the toroidal magnetic field. (d) Approximate toroidal location of mmw system.

≤ 1 s, even though the system can allow for uninterrupted operation at higher power and different kinds of modulation^{15,17}. HWs exit the magnetron through a WR430 rectangular waveguide and are transported to the TORPEX vessel via a transmission line composed of a WR430-to-WR340 waveguide transition, a WR340 waveguide, a step twist and a second WR340 section connected radially at the low field side of the torus (Fig. 1). HWs entering the vessel are expected to be mainly O-mode (with polarization parallel to the magnetic field⁵) with a small X component¹⁷ (perpendicular to the B -field). Given the low first pass absorption of HWs in typical experiments, the initial polarization is anyway expected to be promptly lost due to reflections on the vessel walls¹⁷. As TORPEX is made of stainless steel¹¹, grounded, and closed-off for the most part, HW power is largely confined to the interior of the toroidal vessel. However, the use of dielectric interfaces makes it possible for some HWs to leak out. Specifically, some diagnostics require clear windows which may provide paths of propagation of HWs towards the exterior of the vessel. Among these are the Plexiglas flanges used as vacuum interfaces for the injection and detection of the mmw beam.

Figure 2 shows the mmw system. Millimeter waves of frequency ≈ 30 GHz and power ≈ 10.5 mW are generated with a Gunn-diode source and launched vertically across TORPEX using a pyramidal horn antenna. The waves have X-mode polarization but their dispersion characteristics are very similar to O-mode for the plasmas and B -fields used in our experiments. Detection is performed with an assembly consisting of a pyramidal horn of dimensions $4.2 \text{ cm} \times 5.5 \text{ cm}$ (vertically aligned with the transmission horn) and a WR22 waveguide of length ≈ 22 cm leading to the detector circuitry (Sec. III). The waveguide has a cutoff frequency of 26.35 GHz and blocks any incoming 2.45 GHz waves. Propagation of harmonics

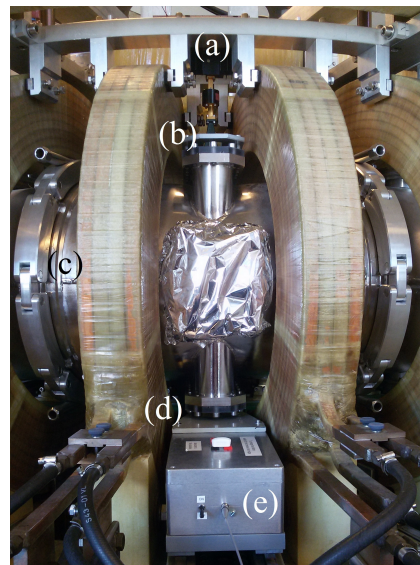


FIG. 2. Millimeter-wave system installed in TORPEX. (a) mmw source. (b) mmws are injected on top through a Plexiglas window using a pyramidal horn. (c) TORPEX vessel and toroidal B -field coils. (d) Second Plexiglas port, receiving pyramidal horn and waveguide. The last two items are hidden from view by the plastic support that fixes the orientation of the antenna directly in front of the transmission horn. (e) Detection system of mmws. There is no direct contact between the system and any metallic surfaces, as the detector rests on an insulating stand. Notice the fiber-optics cable connected in front.

of HW through the waveguide is in principle possible but of no concern, as harmonics of the HWs have negligible power content compared to the expected ~ 1 mW mmws. This observation follows from dedicated measurements of the HW spectral content using a Hewlett-Packard HP-70000 Spectrum Analyzer and an ultra wide bandwidth Vivaldi antenna¹⁸ with S_{11} parameter¹⁹ ≤ -6 dB for the band 2 – 22 GHz. The antenna, which is directly connected to the spectrum analyzer, is placed at the same location and with the same polarization as the mmw receiver horn. Figure 3 shows the EM power at the frequencies of some harmonics for different configurations of HW. Harmonics higher than the third give no signature above noise and are taken to be equivalent to the lowest value compatible with results and noise at lower frequencies. However, we expect their true value to be much lower, assuming power decreases with increasing harmonic number as suggested by PIC simulations²⁰. Thus, we expect < 80 dB of HW harmonic content above the WR22 waveguide cutoff. Assuming the effective area¹⁹ of the Vivaldi antenna to be comparable to that of the horn, we can use the measured ≤ 15 dBm at the fundamental (in all HW configurations) to conclude that at most $-65 \text{ dBm} = 3 \times 10^{-7} \text{ mW}$ of HW power should make it through to the detector. This value is negligible compared to the mmw power.

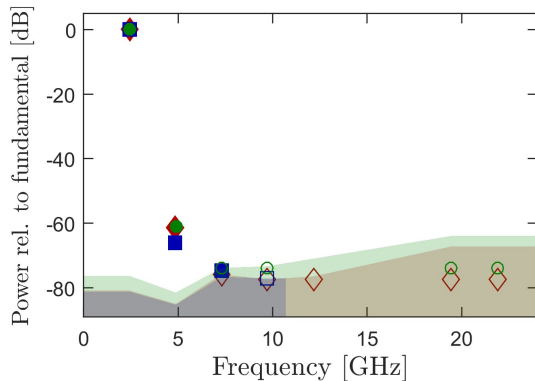


FIG. 3. Power of HW harmonics normalized to the power at the fundamental frequency (≈ 2.45 GHz). Data is taken in three different configurations: $P_{\text{heat}} = 300$ W and *no* plasma (red diamonds), $P_{\text{heat}} = 400$ W and *no* plasma (blue squares), and $P_{\text{heat}} = 400$ W *with* plasma (green circles; see Sec. IV for description of plasma). The shaded areas show the regions where measurements are impossible to distinguish from noise in each configuration (same colors as markers). In other words, the upper boundary of each shaded region corresponds to the observed noise power versus frequency. Solid markers indicate clear observations of harmonics. Hollow markers are used for measurements that gave no signature above noise. We draw them, for reference, at the lowest value compatible with results and noise at lower frequencies.

Spurious HWs can nevertheless be present in areas surrounding the detector system since it is located near a Plexiglas port. These HWs may couple to the detector directly or through connecting cables^{13,14} and produce an unwanted response. Furthermore, there exists a path from the steel vessel to the magnetron through the ground connection, so conductive, capacitive and even radiative¹³ coupling can exist between the magnetron and any circuitry connected to or in proximity of the vessel. Thus, any detection electronics placed in the area must be properly built to avoid situations where noise significantly degrades the signal, as in the case of the original experiments using a bare SDD.

III. OPTICALLY-ISOLATED MMW DETECTOR

To avoid noise coupling, we designed and built an optically-isolated mmw detector (OIMD). Figures 4 and 5 show the system and all its components. The pyramidal horn antenna and WR22 waveguide direct incoming mmws to a Farran Technology zero-bias SDD. The SDD generates a voltage proportional to the power of the mmws^{5,10} (the so called *square-law* regime) which is output through an SMA connector on its back. Connected there is a coaxial cable with a $560\ \Omega$ Resistive Load (RL) between the inner conductor and the shielding chosen to ensure¹⁰ that the SDD remain in the same operating regime for all levels of mmw power expected

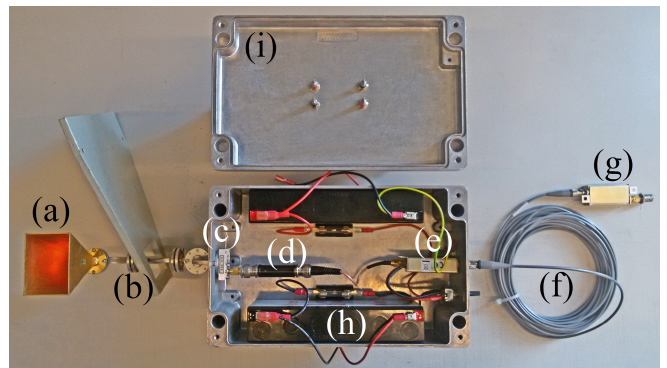


FIG. 4. Picture of the OIMD. (a) Pyramidal horn antenna. (b) WR22 waveguide. The plastic support around it is used to fix the orientation of the antenna during operations (see Fig. 2). (c) Zero-bias SDD. (d) Resistive load (RL). (e) Optical link transmitter. (f) Fiber optics. (g) Optical link receiver. The output of this unit can be connected directly to the data-acquisition system. (h) Two 12 V batteries are used to power the analog-to-optical unit and keep the circuitry isolated. They are shown disconnected only to avoid cable clutter in the image. The optical receiver unit (g) is powered with separate supplies or batteries (not shown). All components in the metallic box are sealed off using the lid (i) during operations (see Fig. 2).

in our experiments (≈ 2 mW). Dedicated measurements for this setup show a sensitivity of -101.3 mV/mW which remains linear up to ≈ 3 mW.

The coax cable goes to the input of an Analog Modules model 732T/R fiber optic link²¹. The link is composed of a transmitter module, which generates an optical signal from the input voltage and sends it through an optical fiber, and a receiver which converts the signal in the fiber back into a voltage. In this way, signals with frequencies DC – 10 MHz can be sent and recovered avoiding all electrical connections. The particular transmitter used in our setup has a $33\ \text{k}\Omega$ input impedance which is a small load compared to the RL, so its insertion has negligible effect on the SDD.

The SDD does not require biasing, but the optical link transmitter does. We use two 12 V, 2.3 Ah lead acid batteries to power the transmitter. The current drawn is ≤ 50 mA so the batteries allow for extended operation times. To avoid large surge currents caused by accidental short circuits, we protect the system with fuses on each battery. There is also a switch to power off the transmitter when not in use, and connectors to recharge the batteries in-situ when the system is installed in TORPEX.

The SDD, RL, optical link transmitter and batteries are all placed in a sealed stainless steel box of wall thickness 3.5 mm. The box is used as ground for all electronics within it but is not connected to the TORPEX ground. There are no open holes that could provide a direct path for mmws or HWs to enter the casing. Indeed, the only

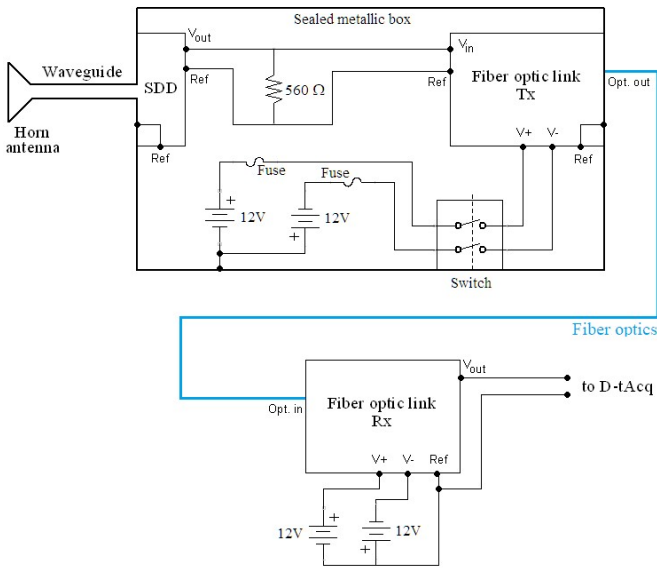


FIG. 5. Schematics of the OIMD showing the different components described in Fig. 4. The voltage references of the SDD and the optical link transmitter are connected internally to their respective casings, which are in direct contact with the metallic box.

holes are those of the waveguide, switch, recharging connectors, and optical fiber which are nonetheless closed off by the corresponding components. A tight lid with a grooved seam precludes a direct line-of-sight towards the interior of the box. Thus, the detection system is heavily isolated from the surrounding electromagnetic environment and it is expected that noise coupling be significantly reduced. This is verified in Sec. IV.

IV. TESTS AND DISCUSSION

In order to determine the performance of the OIMD, we run a series of experiments for different values of P_{heat} using the setup shown in Fig. 2. We compare these observations to a “bare SDD” case, where we remove the optical-isolation and connect the data-acquisition system directly to the output of the RL (Fig. 4d) using a standard $50\ \Omega$ coaxial cable.

In a typical experiment, we activate the mmw source, then the HWs, wait 0.1 s for the magnetron to stabilize, and record 0.2 s of the output of the OIMD, or of the bare SDD, using a 16-bit D-tAcq ACQ196CPCI data acquisition card²² at 250 ksamples/s (the card includes filtering for proper anti-aliasing)¹⁶. Since the SDD operates in square-law regime, the recorded voltage signal is proportional to the detected EM power which, in the absence of noise, is just the mmw power reaching the detector. We use the measured sensitivity of the SDD (including RL; see Sec. III) to obtain the detected power signal $s(t)$ from the recorded voltages. Since the gain of the opti-

cal system is set to *one*, the voltages measured with the OIMD can be converted to power using the same factor.

In the case of the shots taken with a plasma, hydrogen gas is injected in the vessel and an SMT magnetic field (see Sec. II) is set with $B_\phi = 71\ \text{mT}$ (on axis) and $B_z = 2\ \text{mT}$ prior to starting the HWs. This leads to discharges exhibiting turbulence and intermittent structures that can scatter mmws⁸.

We focus on the fluctuations around the mean $\delta s(t) = s(t) - \langle s \rangle_t$, where $\langle s \rangle_t$ is the time average of $s(t)$, to better compare the effect of noise in the signals for the different configurations. For reference, $\langle s \rangle_t \approx 2.2\ \text{mW}$, with a variation $< 5\%$ across all experiments. Figure 6 shows experimental traces of $\delta s(t)$ as well as the computed standard deviation $\sigma(s)$ of $s(t)$. The value of $\sigma(s)$ summarizes the degree of variability of the detected mmw signal and is used to quantify the performance of the system. When the OIMD is present, Fig. 6b shows that $\delta s(t)$ is close to data-acquisition quantization limits (least significance bit) and has noticeably smaller variability compared to the similar situation using a bare SDD. Indeed, Fig. 6c shows that $\sigma(s)$ is very nearly the noise baseline value, independent of P_{heat} , when there is *no* plasma. The situation is very different for the bare SDD, where $\sigma(s)$ increases significantly and has a value that is many times the baseline.

The use of the OIMD is also seen to be very important to distinguish plasma-related variations from noise. This is exemplified by the cases $P_{\text{heat}} = 300 - 600\ \text{W}$ in Fig. 6c, where the use of the OIMD leads to values of $\sigma(s)$ significantly higher than noise when a plasma is present. In comparison, the value of $\sigma(s)$ measured with the bare SDD is similar with plasma and without it.

V. CONCLUSION

We have designed and built an optically-isolated mmw detector system using an SDD, an optical-link and a metallic enclosure that protects mmw detection from being affected by a noisy electromagnetic environment. This is verified in a series of tests that show very good noise immunity over a range of HW power $P_{\text{heat}} \leq 600\ \text{W}$, typical of experiments using plasmas in TORPEX.

The tests also show that use of the OIMD allows distinguishing mmw detection variability due to plasma-related effects, an important prerequisite for experimental studies of propagation of mmws in turbulent plasmas. Indeed, recent measurements and results⁸ show the usefulness of the system and its relevance for future research.

ACKNOWLEDGMENTS

The authors wish to acknowledge the support of the Swiss Plasma Center technical team and in particular of S. Couturier for the assembly of the OIMD. We thank

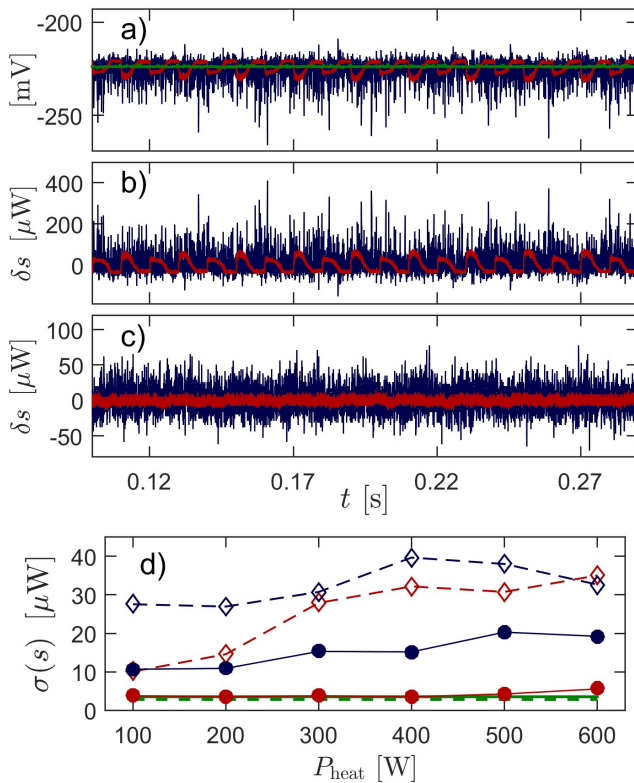


FIG. 6. Experimental observations. (a) Raw voltage signals from bare SDD for no HWs (green) and for $P_{\text{heat}} = 400$ W in the cases with plasma (blue) and without plasma (red). The ≈ 100 Hz signal visible in the red trace stems from pickup as the magnetron is not modulated in our experiments. (b) mmw power fluctuations $\delta s(t)$ corresponding to the data in (a) for active HWs (same color labels). (c) OIMD time trace with (blue) and without plasma (red) for the same value of P_{heat} . Notice the different vertical-axis scale. (d) $\sigma(s)$ for the cases SDD *with* (hollow blue diamonds) and *without* plasma (hollow red diamonds), and OIMD with (solid blue circles) and without plasma (solid red circles). The lines are not fits and are present only to guide the eye. The baseline values of $\sigma(s)$ acquired with no HWs are shown in green for the OIMD (solid line) and the bare SDD (dashed line). The markers at $P_{\text{heat}} = 400$ W correspond to the data shown in (b) and (c).

J-P. Hogge for useful discussions on the characterization of the response of an SDD.

This work has been carried out within the framework of the EUROfusion Consortium and has received funding from the Euratom research and training programme 2014-2018 under grant agreement number 633053. The views and opinions expressed herein do not necessarily reflect those of the European Commission.

This work was supported in part by the Swiss National Science Foundation.

¹S. Wedemeyer, et al., *Solar science with the Atacama Large Mil-*

limeter/Submillimeter Array - A new view of our sun, Space Sci. Rev. 200, 1-73 (2016).

²T.S. Rappaport, Y. Xing, G.R. MacCartney, A.F. Molisch, E. Mellios and J. Zhang, *Overview of millimeter wave communications for fifth-generation (5G) wireless networks with a focus on propagation models*, IEEE Trans. Antennas Propag. 65, 6213-6230 (2017).

³S. Fukao and K. Hamazu, *Radar for meteorological and atmospheric observations*, Springer, Tokyo (Japan), 2014.

⁴F. Töpfer and J. Oberhammer, *Millimeter-wave tissue diagnosis: The most promising fields for medical applications*, IEEE Microwave Magazine 16, 97-113 (2015).

⁵H.J. Hartfuss and T. Geist, *Fusion plasma diagnostics with mm-waves*, Wiley-VCH, Weinheim (Germany), 2013.

⁶S. Alberti, *Plasma heating with millimetre waves*, Nat. Phys. 3, 376 (2007).

⁷A. Köhn, E. Holzhauser, J. Leddy, M.B. Thomas and R.G. Vann, *Influence of plasma turbulence on microwave propagation*, Plasma Phys. Control. Fusion 58, 105008 (2016).

⁸O. Chellaï, S. Alberti, M. Baquero-Ruiz, I. Furno, T. Goodman, F. Manke, G. Plyushchev, L. Guidi, A. Koehn, O. Maj, E. Poli, K. Hizanidis, L. Figini and D. Ricci, *Millimeter-wave beam scattering by field-aligned blobs in simple magnetized toroidal plasmas*, Phys. Rev. Lett. 120, 105001 (2018).

⁹E.V. Sysoeva, F. Silva, E.Z. Gusakov, S. Heuraux and A.Y. Popov, *Electron cyclotron resonance heating beam broadening in the edge turbulent plasma of fusion machines*, Nucl. Fusion 55, 033016 (2015).

¹⁰Agilent Technologies, *Dynamic range extension of Schottky detectors*, Appl. Note 956-5 (1999).

¹¹I. Furno, F. Avino, A. Bovet, A. Diallo, A. Fasoli, K. Gustafson, D. Irajı, B. Labit, J. Loizu, Müller, G. Plyushchev, M. Podestà, F.M. Poli, P. Ricci and C. Theiler, *Plasma turbulence, suprathermal ion dynamics and code validation on the basic plasma physics device TORPEX*, J. Plasma Phys. 81, 345810301 (2015).

¹²A. Fasoli, A. Burckel, L. Federspiel, I. Furno, K. Gustafson, D. Irajı, B. Labit, J. Loizu, G. Plyushchev, P. Ricci, C. Theiler, A. Diallo, S.H. Müller, M. Podestà and F. Poli, *Electrostatic instabilities, turbulence and fast ion interactions in the TORPEX device*, Plasma Phys. Control. Fusion 52, 124020 (2010).

¹³V.P. Kodali, *Engineering electromagnetic compatibility, 2nd ed.*, IEEE Press, Piscataway NJ, 2001.

¹⁴W.K. Brookshier, *Noise signal pickup in coaxial cables*, Nucl. Instr. and Meth. 70, 1-10 (1969).

¹⁵M. Podestà, A. Fasoli, B. Labit, M. McGrath, S.H. Müller and F.M. Poli, *Plasma production by low-field side injection of electron cyclotron waves in a simple magnetized torus*, Plasma Phys. Control. Fusion 47, 19892002 (2005).

¹⁶M. Baquero-Ruiz, F. Avino, O. Chellaï, A. Fasoli, I. Furno, R. Jacquier, F. Manke, and S. Patrick, *Dual Langmuir-probe array for 3D plasma studies in TORPEX*, Rev. Sci. Instrum. 87, 113504 (2016).

¹⁷M. Podestà, *Plasma production and transport in a simple magnetized toroidal plasma*, Ph.D. dissertation (Ecole Polytechnique Fédérale de Lausanne, Switzerland, 2007).

¹⁸P.J. Gibson, *The Vivaldi aerial*, 1979 9th European Microwave Conference, Brighton, UK, 101-105 (1979).

¹⁹C.A. Balanis, *Modern antenna handbook*, John Wiley and Sons, Hoboken NJ, 2008.

²⁰J. Zhang, L. Ying-Hua, Y. Jin-Sheng, C. Le, Y. Wen-Han and X. Wan-Chun, *Research of 2.45GHZ continuous wave magnetron harmonic*, 2009 5th Asia-Pacific Conference on Environmental Electromagnetics, Xian, China, 62-65 (2009).

²¹See <http://www.analogmodules.com/admincenter/datasheets/732tr.pdf> for Analog Modules model 732T/R analog/digital fiber optic link specifications.

²²See <http://www.d-tacq.com/acq196cpci.shtml> for ACQ196CPCI digitizer specifications.